Direct writing of three-dimensional Cu-based thermal flow sensors using femtosecond laser-induced reduction of CuO nanoparticles

S Arakane, M Mizoshiri*, J Sakurai and S Hata
Department of Micro-Nano Systems Engineering, Graduate School of Engineering, Nagoya University 464-8603, Japan

*E-mail: mizoshiri@mech.nagoya-u.ac.jp

Abstract. We have demonstrated the fabrication of two types of thermal flow sensors with Cu-rich and Cu_2O-rich microheaters using femtosecond laser-induced reduction of CuO nanoparticles. The microheaters in the shape of microbridge structures were formed to thermally isolate from the substrates by four layer-by-layer laminations of two-dimensional micropatterns. First, we evaluated the patterning properties such as dispensing coating conditions and degree of reduction for the selective fabrication of three-dimensional Cu-rich and Cu_2O-rich microstructures. Then, a hot-film flow sensor with a Cu-rich microheater and a calorimetric flow sensor with a Cu_2O-rich microheater were fabricated using their respective appropriate laser irradiation conditions. The hot-film sensor with the Cu-rich microbridge single heater enabled us to measure the flow rate in a wide range of 0–450 cc min^{-1}. Although a large temperature dependence of the Cu_2O-rich microbridge heaters caused a large error for the hot-film flow sensors with single heaters, they showed higher heat-resistance and generated heat with a lower drive power. The temperature coefficient of resistance of the Cu_2O-rich microstructures had a semiconductor-like large absolute value and was less than -4.6×10^{-3}°C^{-1}. The higher temperature sensitivity of the Cu_2O-rich microstructures was useful for thermal detection. Based on these advantages, a calorimetric flow sensor composed of the Cu_2O-rich microbridge single heater and two Cu_2O-rich thermal detectors was proposed and fabricated. The calorimetric flow sensor was driven by a circuit for measuring the temperature difference. The Cu_2O-rich flow sensor could detect bi-directional flow with a small output error.

Key words: direct-writing, femtosecond laser, three-dimensional micromachined sensor, thermal flow sensor, laser-induced reduction, CuO nanoparticle

1. Introduction

Three-dimensional (3D) micromachined sensors composed of thermally-isolated heaters and/or thermal detectors have been developed for enhanced performance. These sensors measure properties such as flow, gas and acceleration by calibrating the changes in the sensors' resistance

[1–3]. For example, microbridge heaters in flow sensors are efficiently heated by a low thermal energy transfer to their substrates, resulting in a highly sensitive and responsive measurement of the flow rate achieved using the heater driven by a constant temperature circuit [4]. This type of sensors can detect a wide range of flow values because of their dynamical measurements and are usually called hot-film flow sensors. To detect flow directions, two heaters must be installed in these sensors [5]. Furthermore, using the temperature dependence of the resistance, thermally-isolated detectors also measure the temperature with a high sensitivity and responsivity. Calorimetric flow sensors combining a heater and two thermal detectors at upstream and downstream can correctly detect the flow rate because errors are cancelled using the heater driven by a circuit for the measurement of the temperature difference using the detectors [6,7]. When forward flow is applied to a calorimetric flow sensor, the temperature of the detector located downstream increases, whereas that of the detector located upstream decreases, and vice versa. Thus, calorimetric flow sensors can detect bi-directional flow.

Microheaters are generally formed using metals and semiconductors that are Joule heated by applying the current. In metal microheaters, finer and longer metal patterns such as whorled and raster patterns are formed in order to control their resistance. Semiconductor microheaters can be simpler and smaller than metal microheaters by using them to connect metal electrodes because the resistivity of the semiconductor heater is larger than that of the metal electrodes. Therefore, the semiconductor microheater with large resistance can be efficiently Joule heated by applying an electrical current without elongation of the microheater patterns to increase the resistance. Moreover, semiconductor heaters show a high temperature stability because of their lower current density and lower self-diffusion constants [8]. Therefore, semiconductor microheaters enable the creation of miniaturised thermal-type sensors with lower power consumption.

The microbridge structures in the thermal flow sensors are usually fabricated using conventional 3D microelectromechanical systems (MEMS) technology. However, 3D MEMS technology involves multiple processes such as sputtering, lift-off, and etching. Although some researchers have improved the sensitivities of the thermal flow sensors by combining a metal and a semiconductor [9,10], their fabrication process is more complicated. Thus, as mentioned above, the complexity of the fabrication processes in MEMS, especially the MEMS containing 3D microstructures and various materials, is a long-standing problem.

In contrast, direct-writing technologies have attracted attention as a maskless process that can fabricate complex two-dimensional (2D) and 3D structures using a variety of materials without complicated multi-step processes such as lithography and vacuum deposition methods. For example, in selective laser sintering (SLS) [11,12] and electron-beam melting (EBM) [13,14], 3D bulk metal

structures are created by sintering raw metal powders to form 2D patterns and the layer-by-layer lamination of these patterns. Unfortunately, the application of these methods to the fabrication of 3D microstructures is difficult because it is necessary to use downsized raw metal powders that are easily oxidized during their preparation and setting processes. Meanwhile, inkjet printing has been shown to be suitable for metal micropatterning in printed electronics [15,16]. Although 3D metal microfabrication using this method has been reported [17,18], the materials used for this technique have been restricted to noble metal nanoparticle inks containing precious metals such as Au and Ag, leading to a relatively high fabrication cost.

To overcome these problems, a direct laser-induced reduction of metal oxide (CuO, Cu_2O and NiO) nanoparticles (NPs) has been reported [19,20–22]. In this method, a metal oxide NP solution including metal oxide NPs, a reducing agent, and poly(vinyl pyrrolidone) (PVP), is irradiated by a continuous wave (CW) or nanosecond lasers. 2D Cu and Ni micropatterns are successfully formed by laser-induced reduction, agglomeration, and sintering of oxide NPs. Furthermore, in contrast to the inert atmosphere required for the SLS and EBM techniques, this process can be conducted in air under ambient pressure. The direct-writing process of Cu micropatterns in air by irradiating Cu salt with a CW laser has also been studied by many researchers [23−25]. These methods have been applied to flexible devices such as pressure switches, which were produced by attaching Cu micropatterns on polydimethylsiloxane substrates [23]. We have also previously reported Cu micropatterning using femtosecond laser-induced reduction of the CuO NP solution. Cu-rich and Cu_2O-rich micropatterns exhibiting metal-like and semiconductor-like temperature coefficient of resistance (TCR) values, respectively, have thus far been selectively produced from the same material of CuO NPs by controlling the femtosecond laser scanning speed and pulse energy [26]. Cu is commonly used for electric wiring because of its high conductivity compared with that of Cu_2O. For local Joule heating, the resistance of the microheater must be higher than that of the electrodes. Therefore, the length of Cu_2O microheaters connected with Cu electrodes can be shortened because of their higher resistivity compared with that of the metal electrodes, as previously explained. Moreover, Cu_2O has been studied for application in gas, humidity and temperature sensors because of its large absolute TCR value [27,28]. Based on these studies, Cu_2O-rich sensor components have been fabricated using selective fabrication of Cu-rich and Cu_2O-rich micropatterns, and microtemperature detectors composed of Cu-rich electrodes [29]. In addition, we have demonstrated 3D microfabrication using a combined process of the dispensing coating and the femtosecond laser-induced reduction of CuO NPs [30]. A microbridge heater with four layers was fabricated using Cu-rich micropatterning.

In this study, using femtosecond laser-induced reduction of CuO NPs, we demonstrate the fabrication of two types of thermal flow sensors, namely hot-film and calorimetric flow sensors. First, the conditions of dispensing coating were investigated to obtain the optimal dispensing pressure and pitch. Then, the atomic compositions of the Cu-rich and Cu_2O-rich patterns were investigated. Using these fabrication conditions, a hot-film flow sensor with a Cu-rich microbridge single heater and a calorimetric flow sensor with Cu_2O-rich microheaters and two detectors were fabricated and evaluated.

2. Experimental methods

2.1. Procedures for fabrication of Cu-based microbridge structures

The fabrication process of the Cu-based microbridge structures is as follows. First, the prepared CuO NP solution was dispensing-coated onto a glass substrate (figure. 1(a)). Second, the coated CuO NP solution was irradiated by focused femtosecond laser pulses to form the Cu electrodes (figure. 1(b)). Then, these dispensing coating and laser patterning steps were conducted alternately until the final patterns composed of the electrodes and microbridge heaters were fabricated (figure. 1(c)). Next, the non-reduced CuO NP solution was removed with ethanol to obtain the microbridge structure (figure. 1(d)). Finally, the Cu-based microbridge structure was conformally coated with parylene to protect it from oxidation and deformation (figure. 1(e)). The thickness of the parylene coating was approximately 2 μm.

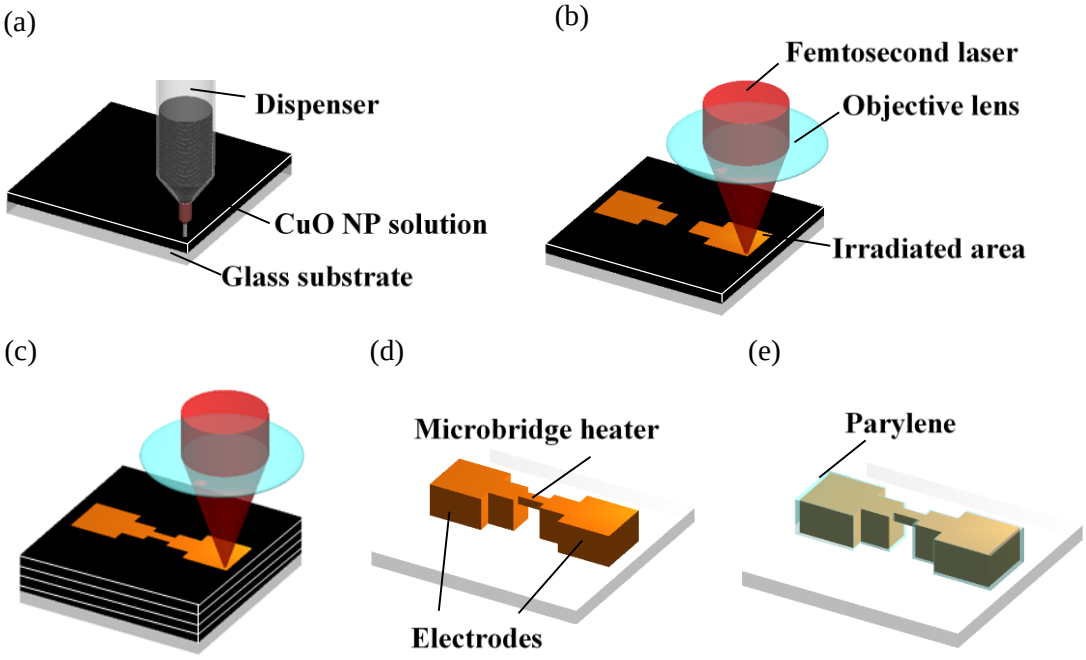

Figure 1. Schematic of the fabrication process for microbridge structures. (a) Dispensing coating CuO NP solution, (b) laser irradiation, (c) dispensing coating CuO NP solution and laser irradiation, repeatedly, (d) removing non-irradiated area and (e) parylene coating.

2.2. Preparation of CuO NP solution

To obtain a uniform solution, ultrasonic waves were used for mixing the materials. First, PVP (Mw ≈ 55000, Sigma-Aldrich) was dissolved into 2-propanol (Wako Pure Chemicals) until the solution became thoroughly transparent. Next, CuO NPs (<50 nm particle size, Sigma-Aldrich) were dispersed into the solution. The concentrations of CuO NPs, 2-propanol, and PVP were 42.1, 41.1 and 16.8 wt%, respectively.

2.3. Dispensing coating and laser scanning system

A dispenser (ML-808GX, Musashi Engineering, Inc.) was used for coating the prepared CuO NP solution with the pressure and inner nozzle diameter of 20–100 kPa and 0.33 mm, respectively. The distance between the substrate or previous layer and the nozzle was fixed to be less than 100 μm.

A femtosecond fibre laser (FemtoFiber pro, Toptica Photonics Co., Ltd) with the pulse duration of 120 fs, repetition frequency of 80 MHz and wavelength of 780 nm was used for direct-patterning. The laser beam was condensed to approximately the spot diameter of 1.2 μm by an objective lens with the numerical aperture of 0.80. The pulse energy of the laser was 0.57 nJ.

XYZ-mechanical stages were used for both dispensing coating and laser irradiation steps. The coating area and laser irradiating area were separately arranged. This setup enabled us to repeatedly carry out the coating of the CuO NP solution and laser patterning without removing the substrate at each step.

2.4. Evaluation methods

The crystal structures of the Cu-based microstructures were examined using an X-ray micro-diffractometer (Rigaku RINT RAPID-S) by Cu-Kα radiation with the X-ray collimator diameter of 0.3 mm. The atomic composition was investigated using scanning electron microscope-energy dispersive X-ray spectrometry (SEM-EDS, Hitachi and Bruker). The thickness of the coated CuO NP solution was measured by white-light interferometry (Canon Zygo). A four-terminal method (Mitsubishi Chemical Analytech Loresta GP) was used to investigate the resistivity of the micropatterns. A power source provided the voltage to a microbridge heater through a connection with silver pastes and enameled wires. The temperature of the microbridge heater was evaluated by infrared thermography (Nippon Avionics Thermo shot F30).

Figure 2 shows the illustration of the measurement setup for the flow sensor. Air was delivered from a compressed gas cylinder in a step state using a three port solenoid valve. The flow rate was calibrated using a commercially available flow sensor (CKD Rapiflow® FSM2). The flow rate was controlled by its regulating valve.

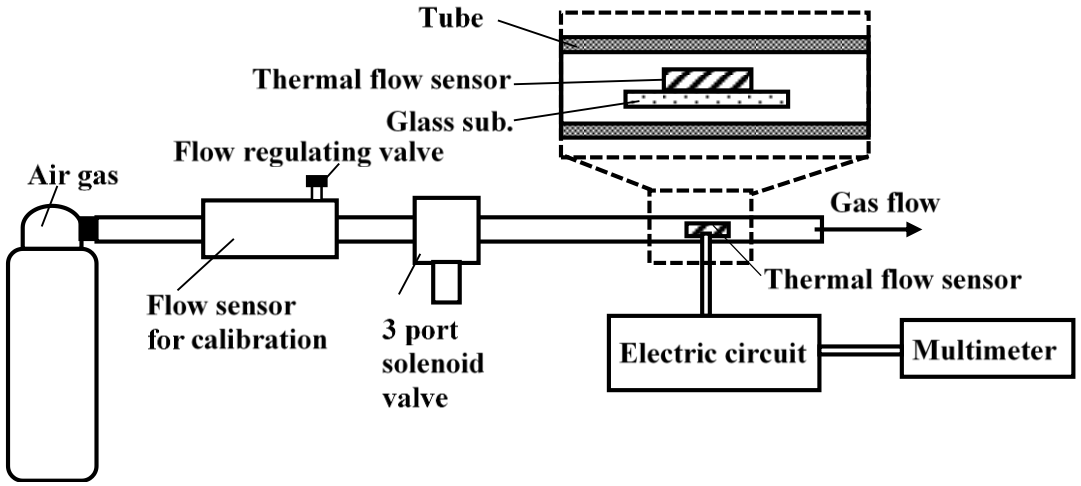

Figure 2. Measurement setup for the thermal flow sensor. The thermal flow sensor was inserted in a tube and calibrated using a commercially available flow sensor.

3. Results and discussion

3.1. Dispensing coating for CuO NP solution

Figure 3 shows the dependence of the thickness and line width of a single line of the CuO NP solution drawn by the dispenser on the dispensing pressure. Both the thickness and line width of the dispensed CuO NP solution increased with increasing pressure. We chose to use 20 kPa, corresponding to the thickness of approximately 12 μm. This value was suitable for conveying the thermal energy to the bottom by laser irradiation. The CuO NP solution was coated by raster scanning with the pitch of 350 μm. According to the results presented in Figure 3, this pitch was sufficiently small to fill the gap between the lines so that uniform CuO NP solution films (thickness ≈ 20 μm) were obtained.

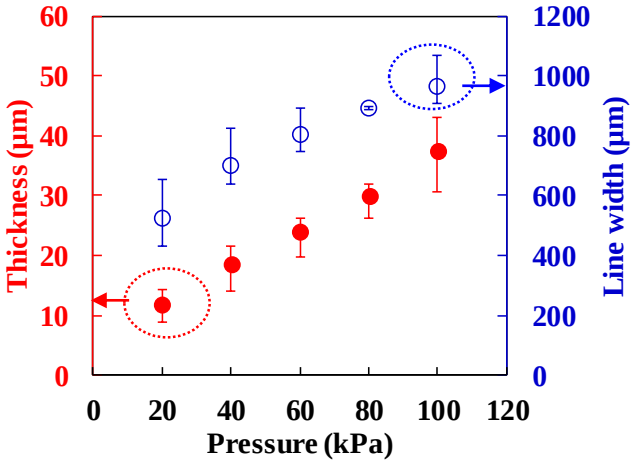

Figure 3. Dependence of the thickness and line width of the single line of CuO NP solution drawn by the dispenser on the dispensing pressure.

3.2. Degree of reduction in the microstructures

The degree of reduction in the microstructures was evaluated using X-ray diffraction (XRD) and EDS. In our previous study, we found that the Cu-rich micropattern can be created at the scanning speed and pitch of 5 mm s^{-1} and 5 μm, respectively [30]. The degree of reduction can be modified by adjusting the laser scanning speed to control the total amount of thermal energy transferred to the CuO NP solution. At the scanning speed of 5 mm s^{-1}, adequate thermal energy was generated to reduce CuO to Cu. The Cu_2O-rich micropattern was also obtained at the scanning speed and pitch of 1 mm s^{-1} and 5 μm, respectively, as shown in figure 4. Following laser irradiation at the scanning speed of 5 mm s^{-1}, the CuO peak intensity decreased and a strong Cu peak intensity appeared. By contrast, the Cu_2O peak intensity increased and the CuO and Cu peak intensities almost disappeared at the scanning speed of 1 mm s^{-1}. These results indicated that the reduced Cu was reoxidized to Cu_2O by the excess thermal energy of the laser irradiation at the scanning speed of 1 mm s^{-1}. On the basis of the XRD results, scanning speeds of 5 mm s^{-1} and 1 mm s^{-1} were used for the Cu-rich and the Cu_2O-rich micropatterning, respectively.

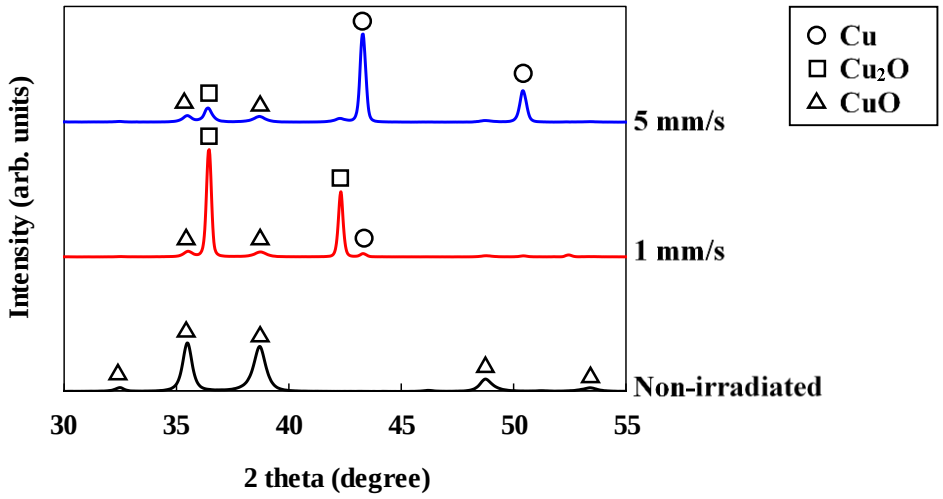

Figure 4. XRD spectra of the CuO NP solution film and micropatterns at scanning speeds of 1 mm s^{-1} and 5 mm s^{-1}.

Figure 5 shows the atomic composition of the Cu-rich and Cu_2O-rich micropatterns. C and Si contributing to PVP and the glass substrate, respectively, were observed. The compositional fractions of Cu and O in the Cu-rich micropattern were higher and lower than in the Cu_2O-rich ones, respectively. This result is consistent with the XRD spectra presented in figure 4.

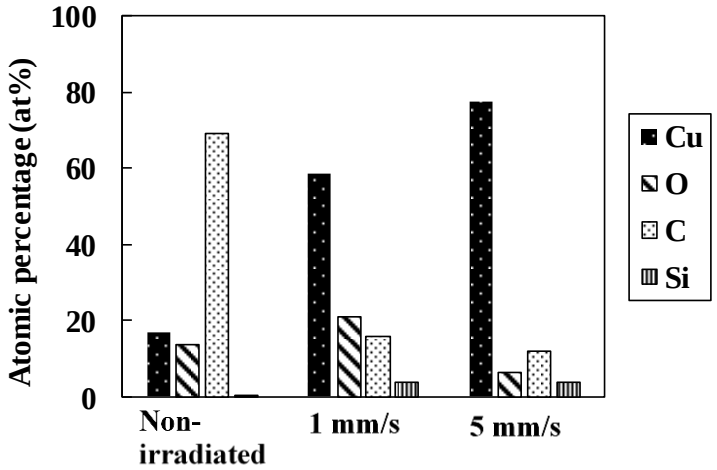

Figure 5. Atomic percentage of the CuO NP solution film and micropatterns at scanning speeds of 1 mm s^{-1} and 5 mm s^{-1}.

The resistivity of the Cu-rich micropattern was 2.0×10^{-5} Ω m, which was approximately 10^4 times larger than the bulk value because of the presence of residual CuO in the micropatterns [30]. Such a higher resistivity is advantageous because it enables the heater to be smaller and

simpler than the heaters created by MEMS. The resistivity of the Cu_2O-rich micropattern was 2.0 Ω m, approximately equal to the corresponding bulk value [31].

3.3. Hot-film sensor with Cu-rich microbridge single heater

We have demonstrated a hot-film flow sensor with the Cu-rich microbridge single heater. The ability to detect the flow rate dynamically in a wide range of values is an advantage of the hot-film flow sensors driven with a constant temperature circuit. Figures 6(a) and 6(b) show a schematic and an optical microscope image of the Cu-rich microbridge structure composed of 1st–4th layer electrodes and fourth layer microbridge heater. The Cu-rich microstructure was formed at the scanning speed of 5 mm s^{-1}. The space underneath the microbridge heater which was expected to work as the thermal isolation from the substrate was observed in an SEM image (figure 6(c)). Owing to this thermally insulating space, the application of a voltage only generated heat at the fourth layer of the microbridge heater, as shown in the infrared image (figure 6(d)).

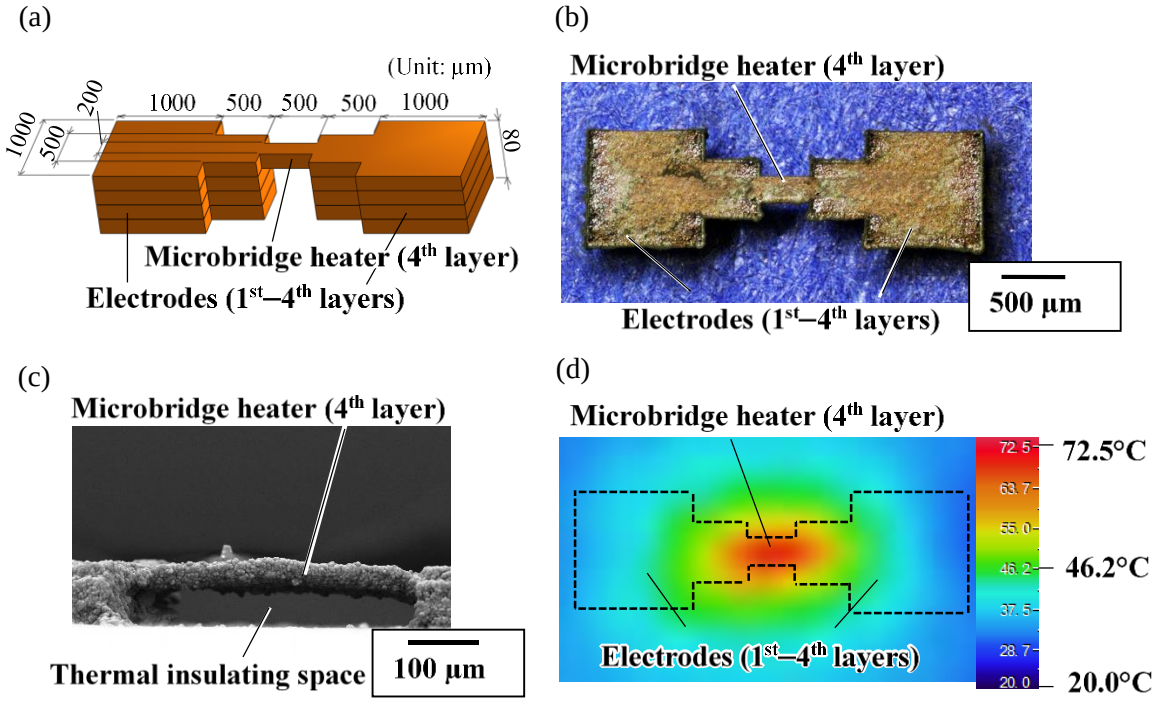

Figure 6. (a) Schematic and (b) optical microscopy image of the Cu-rich microbridge structure. (c) SEM image of the Cu-rich microbridge heater with thermal insulating space. (d) Infrared image of the Cu-rich microbridge structure at an applied voltage of 0.7 V.

The characteristics of the Cu-rich microbridge heater were evaluated. Figure 7(a) shows the dependence of the current of the Cu-rich microbridge structure on the applied voltage. Figure 7(b) shows the dependence of the temperature of the Cu-rich microbridge heater on the drive power.

The Cu-rich microheaters were disconnected at approximately 110°C, which may be caused by local overheating because of the existence of voids in the microstructures. Therefore, we applied a voltage until the temperature of approximately 70°C in order to prevent the disconnection of the microheaters. The hysteresis of these characteristics was significantly small, indicating that the microbridge heater could work without any deformation and oxidation during heating. Cu-rich microbridge structure was constantly heated at 60°C in the flow rate measurement. The TCR of the Cu-rich microbridge structure was investigated in an oven, and its value was found to be approximately 1.2×10^{-3}°C^{-1}.

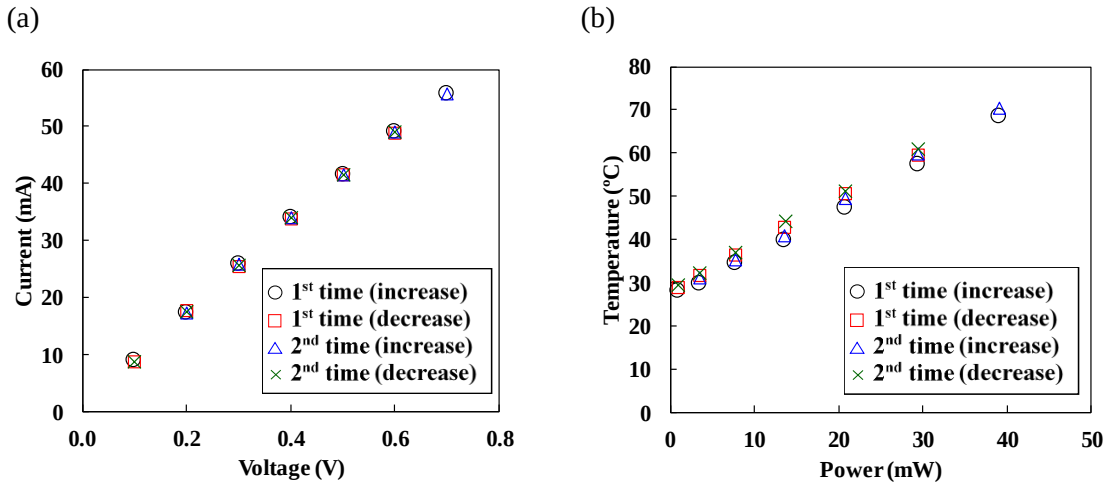

Figure 7. (a) Applied voltage vs current of the Cu-rich microbridge structure. (b) Drive power vs temperature of the Cu-rich microbridge heater. The applied voltage was increased and decreased two times.

The hot-film sensor was demonstrated for measuring the flow rate in a tube. Figure 8(a) shows the image of the Cu-rich flow sensor inserted in the tube. The dependence of the sensor output on the flow rate is shown in figure 8(b). The flow rate was varied in the 0–450 cc min^{-1} range and was increased and decreased four times in order to investigate the precision of this flow sensor. The calibration curve of the sensor output in hot-wire and hot-film sensors is obtained using the equation:

$$V^2 = A + BU^n \tag{1}$$

where V is the sensor output and U is the flow velocity. A, B and n are constants. This equation is based on King's law [32]. Based on this equation, the sensitivity of the sensor output depends on B and n. When the wire is infinitely long, n is generally 0.5. However, n in this measurement shifted from 0.5 because the length of the wire was finite. The curve fitted using King's law is shown in figure 8(b). Despite a slight variation, the sensitivity in the Cu-rich flow sensor is equal to or greater

than that of a flow sensor fabricated using MEMS technology [33]. The maximum root mean square error of the sensor output (V) in this measurement was 11 mV at 450 cc min^{-1}. The error was generated because this sensor was easily affected by the disturbance from the environment, so that adding a temperature-compensating resistance was expected to decrease the error. The 0–90% rise and fall times of the sensor outputs were approximately 2.0 s and 2.2 s, respectively, relatively slower than those of the sensors fabricated by MEMS technology [4]. The slower rise and fall times are because of the heat spreading to the electrodes (figure 6(d)). Therefore, this slower response time can be improved by miniaturizing the electrodes.

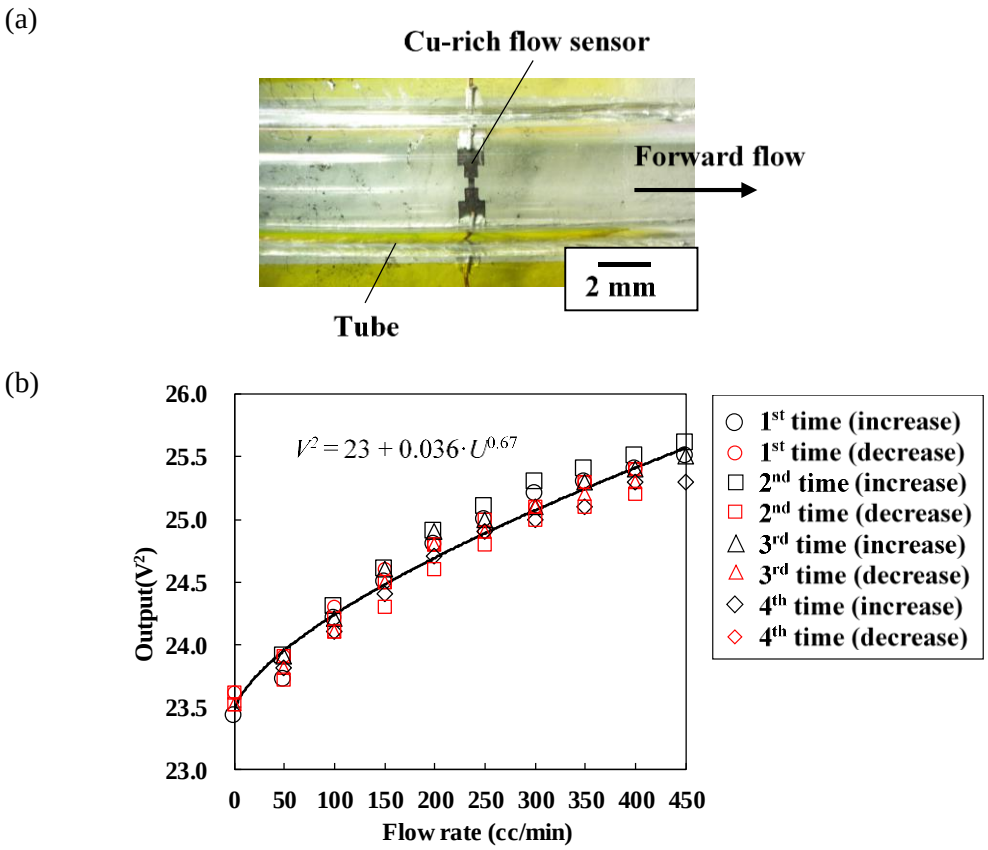

Figure 8. (a) Optical microscopy image of a Cu-rich flow sensor inserted in a tube using the concept of a hot-film sensor. Only forward flow was applied to this sensor. (b) Dependence of sensor output of the Cu-rich flow sensor on the flow rate. The one-directional flow rate was increased and decreased four times in the range of 0–450 cc min^{-1}.

3.4. Calorimetric flow sensor with Cu_2O-rich microbridge single heater and two detectors

We attempted to fabricate a hot-film flow sensor with Cu_2O-rich microbridge single heater following a procedure similar to that used for the fabrication of the Cu-rich microbridge single heater. However, when the single Cu_2O-rich microbridge heater was operated as a hot-film flow

sensor, the sensor output was not stable because the sensor was easily influenced by the ambient temperature because of its higher TCR.

In contrast, the low thermal conductivity of the Cu_2O microstructures is advantageous for heaters, enabling efficient conversion of electrical energy to thermal energy with lower driven power. Furthermore, the higher temperature sensitivity of the Cu_2O microstructures was effective for temperature detection. In a previous study, we have found that Cu_2O-rich micropatterns exhibited a high temperature sensitivity [26]. To exploit these advantages, we proposed a calorimetric flow sensor composed of a Cu_2O-rich microbridge single heater and two detectors. Figures 9(a) and 9(b) show a schematic and optical microscope image of the flow sensor with the Cu_2O-rich microbridge structures. Although the Cu_2O-rich microbridge heater was thicker than its Cu-rich analogue because of the greater amount of thermal energy irradiated at the slower scanning speed, the Cu_2O-rich microbridge structures also had thermal insulating spaces underneath the microbridge heaters (figure 9(c)). The structures were composed of 1^{st}–4^{th} layer Cu-rich electrodes and fourth layer Cu_2O-rich microbridge heaters. The middle and both sides of the microbridge structures were used as the heater and temperature detectors, respectively. Figure 9(d) shows the infrared image of the Cu_2O-rich microbridge structure at the applied voltage of 20 V. We found that the Cu_2O-rich microbridge structure also generated heat only at the microbridge heater.

(a)

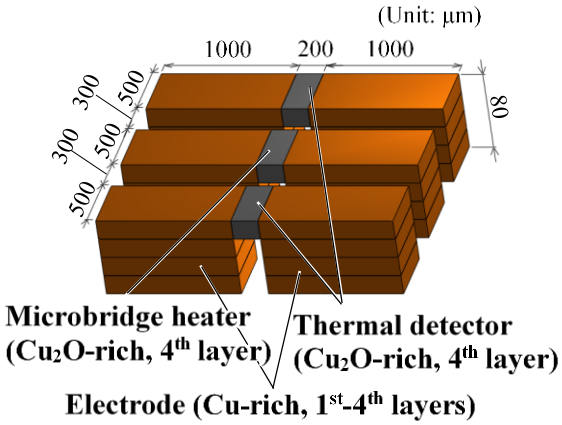

(b)

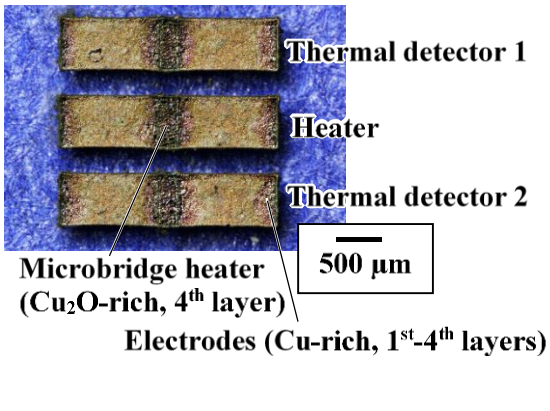

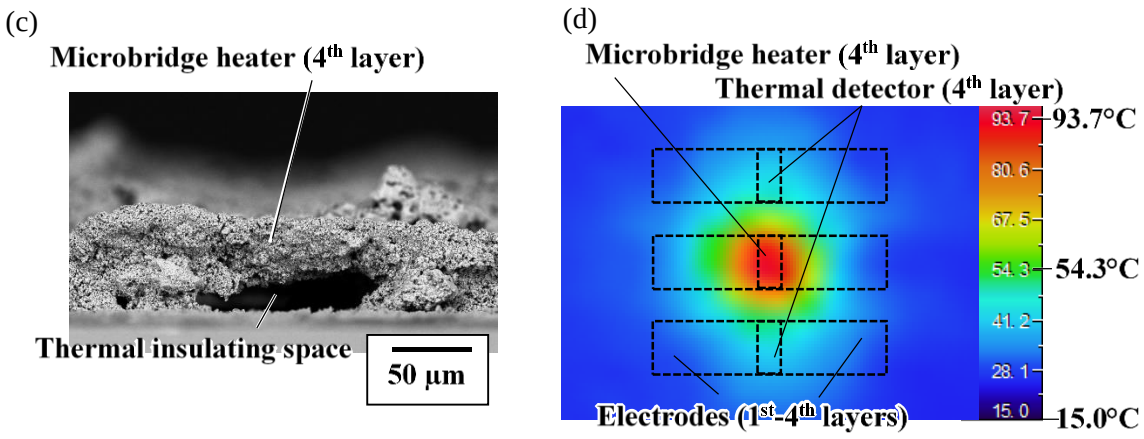

Figure 9. (a) Schematic and (b) optical microscopy image of the Cu_2O-rich microbridge structures. The middle of the microbridge was used as a heater and the sides were used as temperature detectors. (c) SEM image of the Cu_2O-rich microbridge heater with thermal insulating space. (d) Infrared image of the Cu_2O-rich microbridge structure at an applied voltage of 20 V.

The characteristics of the Cu_2O-rich microbridge heater are shown in figures 10. The Cu_2O-rich microbridge heater was disconnected at approximately 240°C, at much higher temperature than the Cu-rich microbridge. Furthermore, the power consumption of the Cu_2O-rich microbridge heater was lower than that of the Cu-rich microbridge because the semiconductor-like Cu_2O-rich material shows lower self-thermal diffusion. Thus, the Cu_2O-rich microbridge exhibited higher performance as a heater than the Cu-rich microbridge. A constant voltage of 20 V corresponding to approximately 95°C was applied to the microbridge heater to heat both sides of the temperature detectors. The TCR values of the temperature detectors were $-6.8 \times 10^{-3}°C^{-1}$ and $-4.6 \times 10^{-3}°C^{-1}$, respectively. These negative TCR values indicated that the Cu_2O-rich microbridge structures shows semiconductor-like TCR, as we have reported previously [26]. The difference between the TCR values of the two temperature detectors arises because the laser beam was sometimes defocused on the surface of the CuO NP solution film because of its surface roughness, making it difficult to always obtain materials with completely consistent properties.

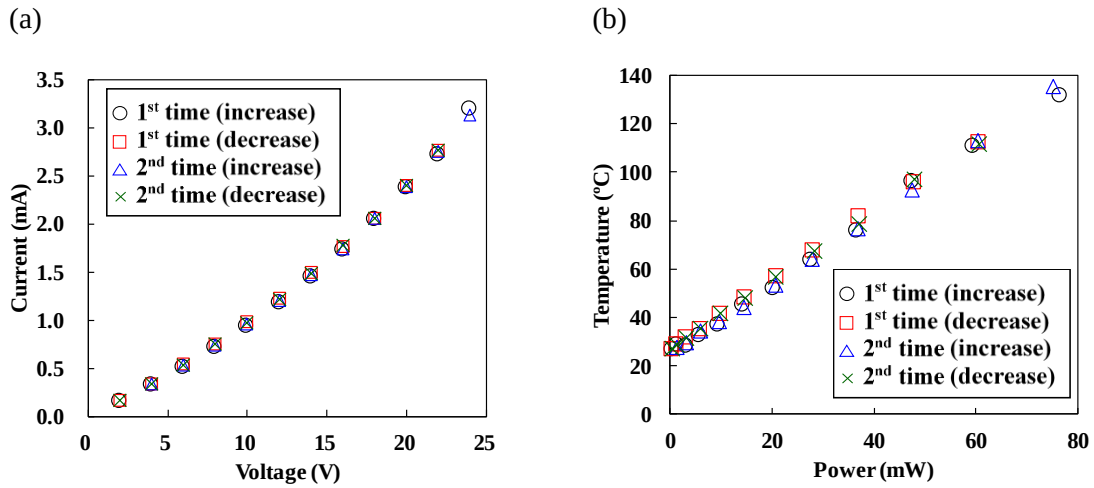

Figure 10. (a) Applied voltage vs current of the Cu_2O-rich microbridge structure. (b) Drive power vs temperature of the Cu_2O-rich microbridge heater. The applied voltage was increased and decreased two times.

Figure 11(a) shows the Cu_2O-rich flow sensor inserted in a tube. The resistance of both sides of the microbridge structures varied with the asymmetric temperature distribution created by the heater with the flow. The resistance difference was evaluated with a Wheatstone bridge and was amplified by an operational amplifier. The sensor output with the forward and backward flows was estimated as shown in figure 11(b). The flow was increased and decreased in both directions four times in the 0–150 cc min^{-1} range. The flow directions were switched by changing the direction of the tube attachment. It was found that the sensor output increased by increasing the forward flow rate. Conversely, the sensor output decreased with an increase of the backward flow rate. When the flow rate was 150 cc min^{-1} or higher, the output became constant because of the constant temperature distribution between the two detectors. To evaluate the sensitivity of the Cu_2O-rich flow sensor, the sensitivity at zero flow (S_0) was utilised [34]:

$$S_0 = \left.\frac{dV}{dQ}\right|_{Q\to 0} \tag{2}$$

where V is the sensor output and Q is the flow rate. When a polynomial fitting curve was applied to the sensor output, the sensitivities at zero flow of the Cu_2O-rich flow sensor for forward and backward flows were 1.1 and 0.66 mV (cc min^{-1})$^{-1}$, respectively. These values were much greater than those of a sensor fabricated using MEMS technology for a similar measurement range (i.e. 0.0029 mV (cc min^{-1})$^{-1}$) [34]. This increased sensitivity was observed because the semiconductor-like a larger absolute value of TCR generated larger change in resistance between the two

temperature detectors. The maximum root mean square errors value of the sensor output in the Cu_2O-rich flow sensor at the forward and backward flows were 4.3 mV and 5.0 mV, respectively, lower than that of the Cu-rich microbridge. Hence, although the measurement range was smaller than that used for the Cu-rich flow sensor, the Cu_2O-rich flow sensor accurately detected bi-directional flow. These errors can be decreased further by decreasing the TCR gap between the two temperature detectors.

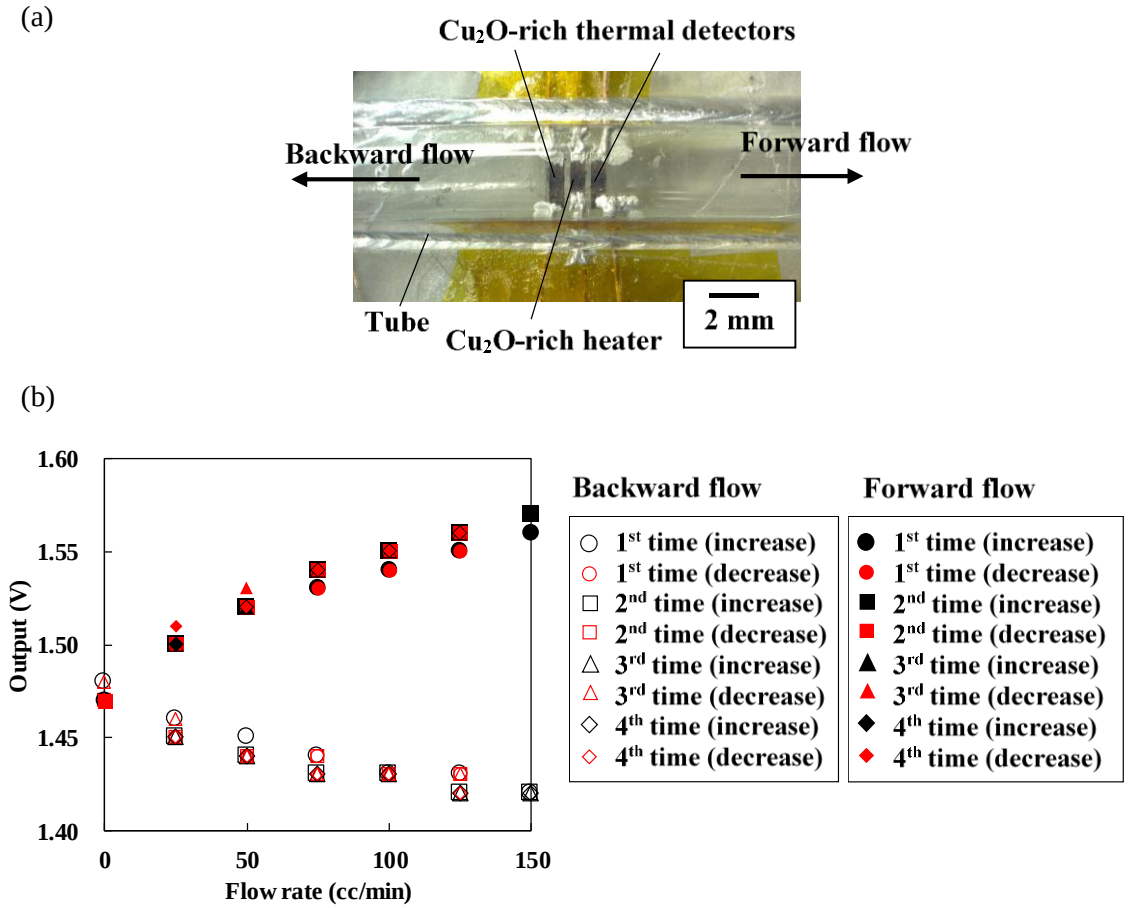

Figure 11. (a) Optical microscopy image of the Cu_2O-rich flow sensor inserted in a tube using the concept of calorimetric sensors. The forward and backward flows were applied to this sensor. (b) Dependence of sensor output of the Cu_2O-rich flow sensor on the flow rate. The bi-directional flow rate was increased and decreased four times in the range of 0–150 cc min^{-1}.

4. Conclusion

We have demonstrated thermal flow sensors fabricated by the femtosecond laser-induced reduction of CuO NPs.

(1) The conditions of dispensing coating were evaluated. Uniform CuO NP solution films (thickness ≈ 20 μm) were obtained at the dispensing pressure and raster scanning pitch of 20 kPa and 350 μm, respectively.
(2) The degree of reduction was investigated using XRD and EDS. The XRD and EDS results were consistent and showed that Cu-rich and Cu_2O-rich micropatterns were selectively fabricated by controlling the scanning speed.
(3) The single Cu-rich microbridge structure was used for a hot-film flow sensor with a constant temperature circuit. The Cu-rich flow sensor could detect a wider range of flow values than the Cu_2O-rich one. The relationship between the flow rate and sensor output was fitted to the King's law model.
(4) The calorimetric flow sensor composed of a Cu_2O-rich microbridge heater and temperature detectors was also demonstrated. The Cu_2O-rich flow sensor could detect bi-directional flows and its output error was small.

The direct-writing process of 3D metal and semiconductor microstructures not relying on the conventional complicated methods demonstrated in this study is useful for the fabrication of prototype devices.

Acknowledgments

This study was partially supported by the Nanotechnology Platform Program (Micro-Nano Fabrication) of the Ministry of Education, Culture, Sports, Science and Technology, Japan (MEXT) and by the Cross-ministerial Strategic Innovation Promotion Program (SIP) of the New Energy and Industrial Technology Development Organization (NEDO).

References

[1] Nguye N T 1997 *Flow Meas. Instrum.* **8** 7

[2] Ho J J, Fang Y K, Wu K H, Hsieh W T, Chen C H, Chen G S, Ju M S, Lin J J, Hwang S B 1998 *Sens. Actuators* B **50** 227

[3] Mailly F, Giani A, Martinez A, Bonnot R, Temple-Boyer P and Boyer A 2003 *Sens. Actuators* A **103** 359

[4] Shikida M, Kim P and Shibata S 2016 *Microsyst Technol* doi:10.1007/s00542-016-3168-9

[5] Shikida M, Yokota T, Naito J and Sato K 2010 *J. Micromech. Microeng.* **20** 055029

[6] Dijkstra M, de Boer M J, Berenschot J W, Lammerink T S J, Wiegerink R J and Elwenspoek M 2008 *Sens. Actuators* A **143** 1

[7] Johnson R G and Egashi R E 1987 *Sens. Actuators* A **11** 63

[8] Spannhake J, Schulz O, Helwig A, Krenkow A, Müller G and Doll T 2006 *Sensors* **6** 405

[9] Kohl F, Fasching R, Keplinger F, Chabicovsky R, Jachimowicz A and Urban G 2003 *Measurement* **33** 109

[10] Glaniger A, Jachimovicz A, Kohl F, Chabicovsky R and Urban G 2000 *Sens. Actuators* A **85** 139

[11] Tang Y, Loh H T, Wong Y S, Fuh J Y H, Lu L and Wang X 2003 *J. Mater. Process. Technol.* **140** 368

[12] Kathuria Y P 1999 *Surf. Coatings Technol.* **643** 116

[13] Cormier D, Harrysson O and West H 2004 *Rapid Prototyp. J.* **10** 35

[14] Heinl P, Rottmair A, Körner C and Singer R F 2007 *Adv. Eng. Mater.* **9** 360

[15] Lee H H, Chou K S and Huang K C *2005 Nanotechnology* **16** 2436

[16] Perelaer J, Hendriks C E, de Laat A W M and Schubert U S 2009 *Nanotechnology* **20** 165303

[17] Fuller S B, Wilhelm E J and Jacobson J M 2002 *J. Microelectromech. Syst.* **11** 54

[18] Ko S H, Chung J, Hotz N, Nam K H and Grigoropoulos C P 2010 *J. Micromech. Microeng.* **20** 125010

[19] Kang B, Han S, Kim J, Ko S and Yang M 2011 *J. Phys. Chem*. C **115** 23664

[20] Lee H and Yang M 2015 *Appl. Phys.* A **119** 317

[21] Lee D, Paeng D, Park H K and Grigoropoulos C P 2014 *ACS Nano* **8** 9807

[22] Paeng D, Lee D, Yeo J, Yoo J H, Allen F I, Kim E, So H, Park H K, Minor A M and Grigoropoulos C P 2015 *J. Phys. Chem.* C **119** 6363

[23] Bai S, Zhou W, Hou T, and Hu A 2016 *Journal of Laser Micro/Nanoengineering* **7** 333

[24] Kordás K, Bali K, Leppävuori S, Uusimäki A and Nánai L 2000 *Appl. Surf. Sci.* **154–155** 399

[25] Manshina A A, Povolotsky A V, Ivanova T U, Tver'yanovich Y S, Tunik S P, Kim D, Kim M and Kwon S C 2007 *Applied Physics* A **89** 755

[26] Mizoshiri M, Arakane S, Sakurai J and Hata S 2016 *Appl. Phys. Express* **9** 036701

[27] Shishiyanu S T, Shishiyanu T S and Lupan O I 2006 *Sens. Actuators* B **113** 468

[28] Kevin M, Ong W L, Lee G H and Ho G W 2011 *Nanotechnology* **22** 235701

[29] Mizoshiri M, Ito Y, Arakane S, Sakurai J and Hata S 2016 *Jpn. J. Appl. Phys* **55** art. no. 06GP05.

[30] Arakane S, Mizoshiri M, Sakurai J and Hata S 2017 *Appl. Phys. Express* **10** 017201

[31] Mathew X, Mathews N R and Sebastian P J 2001 *Sol. Energy Mater. Sol. Cells* **70** 277

[32] King L V 1914 *Phil. Trans. R. Soc.* A **214** 373

[33] Shikida M, Naito J, Yokota T, Kawabe T, Hayashi Y and Sato K 2009 *J. Micromech. Microeng.* **19** 105027

[34] Palmer K, Kratz H, Nguyen H and Thornell G 2012 *J. Micromech. Microeng.* **22** 065015